JPL Publication D-111714

MODIS/ASTER (MASTER) Airborne Simulator

Level-3 Evapotranspiration L3 (ET) Algorithm Theoretical Basis Document

Madeleine Pascolini-Campbell, Alberto Candela Garza, Gerardo Rivera, Simon Hook

MASTER Science Team
Jet Propulsion Laboratory
California Institute of Technology

January 2026
Document no. D-111714

National Aeronautics and Space Administration

Jet Propulsion Laboratory

- Madeleine Pascolini-Campbell
  Mailstop 183-506A
  Jet Propulsion Laboratory
  4800 Oak Grove Dr.
  Pasadena, CA 91109
  Email: madeleine.a.pascolini-campbell@jpl.nasa.gov

List of Acronyms

ATBD	Algorithm Theoretical Basis Document
ECOSTRESS	ECOSystem Spaceborne Thermal Radiometer Experiment on Space Station
ET	Evapotranspiration
G	Ground Heat Flux
GEOS-FP	Goddard Earth Observing System - Forward Processing
HyTES	Hyperspectral Thermal Emission Spectrometer
L-1	Level 1
L-2	Level 2
L-3	Level 3
LST	Land Surface Temperature
LSTE	Land Surface Temperature and Emissivity
LWIR	Longwave Infrared
MASTER	MODIS/ASTER Airborne Simulator
MERRA-2	Modern-Era Retrospective Analysis for Research and Applications - 2
MWIR	Midwave Infrared
NDVI	Normalized Difference Vegetation Index
RH	Relative Humidity
SEB	Surface Energy Balance
STIC	Surface Temperature Initiated Closure
SWIR	Shortwave Infrared
VNIR	Visible-and-Near Infrared

Table of Contents

Figures

Tables

1. Introduction

1.1. Background

Evapotranspiration (ET) represents the flux of water transferred from the land surface to the atmosphere from soils and plants. The rate of ET is controlled by many environmental and biological variables including: incoming radiation, the atmospheric water vapor deficit, soil water availability, and vegetation physiology and phenology (Brutsaert, 1982; Monteith, 1965; Penman, 1948). LST exerts control on plant transpiration, with higher temperatures leading to plants to close their stomata to conserve water. LST is therefore important in the estimation of ET. ET is a Level-3 (L-3) product constructed from a combination of the MASTER Level-1 (L-1) Radiance, and Level-2 (L-2) Land Surface Temperature (LST) and Emissivity (LSTE) product and auxiliary meteorology data. Since the MASTER instrument measures 50 spectral channels spanning the visible to longwave infrared (LWIR), it is possible to obtain concurrent LST, albedo and normalized difference vegetation index (NDVI) which is needed in ET estimation, making it an ideal instrument for observing ET. We use the Surface Temperature Initiated Closure (STIC) model to estimate ET, given it directly includes LST into the estimation of surface wetness (Mallick et al., 2015; 2018).

1.2. Purpose

In this ATBD, we provide:

1. Background on the MASTER instrument.
2. Description of the ET parameter characteristics and requirements;
3. Description of the general form of the ET algorithm in the MASTER product workflow;
4. Auxiliary data products;
5. Plan for the calibration and validation (Cal/Val) of the ET retrieval.

2. Parameter Description and Requirements

2.1. Attributes of the ET data produced by MASTER:

- Spatial resolution depends on altitude of the airborne platform and varies from 5 m to 50 m (Table 1 for aircraft details);
- Temporal resolution depends on the airborne acquisition schedule and campaign;
- Latency as required;

3. MASTER - Instrument Characteristics

3.1. Radiometer

As described in Hook et al., (2001) - The MASTER instrument was developed by the NASA Ames Research Center in conjunction with the Jet Propulsion Laboratory. It consists of three key components: a scanning spectrometer, a digitizer, and a data storage system. The scanning unit was built by Sensys Technology (formerly Daedalus Enterprises), while the digitizer and data storage system was a collaborative effort between Berkeley Camera Engineering and the Ames Airborne Sensor Facility (ASF), which also managed the system integration

MASTER supports a variety of scan speeds, allowing the acquisition of contiguous imagery from different altitudes and with varying pixel sizes (Table 1). The optical system includes a spectrometer mounted on a scanning fore-optic unit. Both the spectrometer and fore-optics portions are mated to an optical baseplate. The fore-optics employ a 45° rotating scan mirror that directs light into a Gregorian telescope, through a series of mirrors and apertures, and finally into the spectrometer.

The spectrometer separates incoming radiation into four wavelength regions – visible-infrared (VIR), shortwave-infrared (SWIR), mid-infrared (MIR) and thermal infrared (TIR) – using dichroic beam slitters. Each region is dispersed by a diffraction grating onto its own detector

array. The system design ensures high optical efficiency and radiometric uniformity across the field of view. Electrical signals from the detectors are amplified, digitized through adaptive 16-bit converters, and stored along with navigation and engineering data. The use of actively controlled preamplifiers and optical isolation minimizes noise and calibration drift, ensuring high radiometric accuracy. Further details of the optical system are given in King et al. (1996).

Table 1: MASTER sensor - Summary Characteristics

Summary characteristics	
Wavelength Range (µm)	0.4 - 13
Number of channels	50
Number of pixels	716
Instantaneous field of view	85.92°
Platforms	DOE King Air Beachcraft B200; NASA ER-2; NASA DC-8
Pixel size DC-8 (m)	10 – 30
Pixel size NASA ER-2 (m)	50
Pixel size DOE King Air Beachcraft B200 (m)	5 – 25
DC-8 range – without refueling	5403 statute miles
ER-2 range – without refueling	3700 statute miles
B200 range – without refueling	700 statute miles
Scan speed	6.25/12/5/25 rps
Calibration VIS-SWIR	Laboratory Integrating Sphere
Calibration MIR-TIR	2 on-board blackbodies
Data Format	Hierarchical Data Format (HDF)
Digitalization	16-bit
Products	
Level 1B	Radiance at sensor
Level 2	Emissivity and Land Surface Temperature
Level 3	Surface Mineralogy Analysis
	Evapotranspiration
	Elevated Temperature Feature
	Fire Radiative Power

3.2 Band positions

MASTER - airborne sensor - acquires multispectral data across the visible-to-shortwave infrared (VSWIR) to TIR region using 50 channels ranging from 0.4 to 13 microns. The spectral configuration, listed in Table 2, is divided into 4 regions: VIS (channels 1-11); SWIR (channels 12-25); MIR (channels 26-40); TIR (channels: 41-50). The TIR includes channels in the wavelength range: 7.7-12.9 micron, providing continuous coverage of the atmospheric window and enabling detailed analysis of surface thermal properties. The center wavelength position and width of each band – width-at-half-maximu (FWHM) – are defined by the geometry of the grating-based spectrometer and are calibrated before and after each major flight campaign. Therefore, small shifts in channel center positions may occur between calibration cycles and the calibration closest to the acquisition date should be used when performing quantitative spectral analyses.

In the current MASTER Thermal and Emissivity Separation (TES) algorithm (Gillepsie et al., 1998), only atmospheric window bands are used to retrieve spectral emissivity and the land surface temperature. These include band 43 (8.61 μm), 44 (9.05 μm), 47 (10.62 μm), 48 (11. 31μm), and 49 (12.11 μm) – see Figure 1. MASTER Band 42 (8.18 μm) falls within the strong water absorption band located at 6.3 μm (ν_2 bending mode) where atmospheric transmissivities can decrease below 60% for high water vapor conditions. MASTER band 50 (12.84 μm) falls within the water vapor rotation band that extends beyond 12 μm and is also not included in TES for that reason. Currently we do not have the necessary accuracy, nor spatial resolution in water vapor profiles used to atmospherically correct thermal infrared data for these two bands, that could result in large uncertainties in LST&E retrievals from TES exceeding 2 K in LST and 2.5% in emissivity. Similarly, MASTER band 45 (9.68 μm) and band 46 (10.08 μm) are not used in TES because they fall within the strong ozone (O_3) absorption centered around 9.6 μm (the ν_3

asymmetric stretch vibration band). In this region atmospheric transmittances can range between 20-40% resulting in very little surface radiance reaching the sensor and resulting in large LST&E errors and noisy retrievals.

It is expected that small adjustments to the band positions, widths, and transmission will be made based on ongoing engineering filter performance capabilities and finalized once the filters are fabricated.

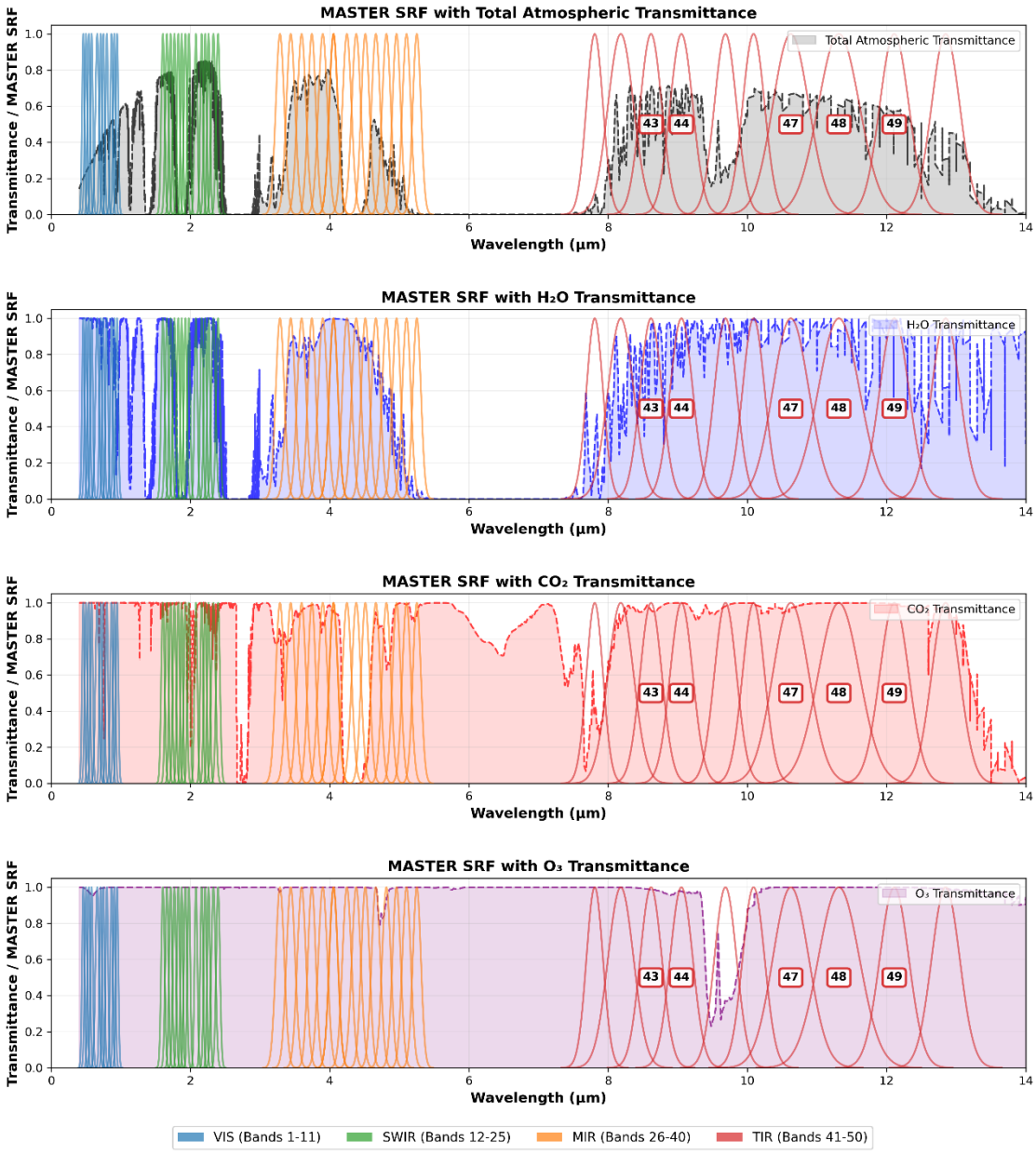

Figure 1: MASTER Spectral Response Function (September 2025). 50 bands: 11 in the VNIR (light blue); 14 in the SWIR (green); 15 in the MIR (orange); and 10 in the TIR (red). MASTER SRF is plotted against the atmospheric transmittance. From the bottom: O3 transmittance (purple); CO2 transmittance (red); H2O transmittance (blue); total transmittance (grey).

Table 2: MASTER SRF based on the 2025 campaign - Date of Calibration: Sep 2025; location: NASA Aims.

More details at: https://asapdata.arc.nasa.gov/sensors/master/data/srf/Sep_25_srf.html

	Band#	halfpp	halfpp	FWHM	center	peak
VIR – 1	1	0.439	0.4802	0.0412	0.4596	0.46
VIR – 2	2	0.4758	0.5209	0.0451	0.4984	0.5
VIR – 3	3	0.5193	0.5624	0.0431	0.5409	0.542
VIR – 4	4	0.5598	0.601	0.0412	0.5804	0.58
VIR – 5	5	0.6303	0.6901	0.0598	0.6602	0.652
VIR – 6	6	0.6895	0.7307	0.0412	0.7101	0.71
VIR – 7	7	0.7293	0.7698	0.0405	0.7495	0.75
VIR – 8	8	0.7788	0.8193	0.0406	0.7991	0.8
VIR – 9	9	0.8445	0.8857	0.0412	0.8651	0.866
VIR – 10	10	0.8848	0.9257	0.0408	0.9053	0.906
VIR – 11	11	0.9251	0.9669	0.0418	0.946	0.946
SWIR – 1	12	1.5757	1.6317	0.056	1.6037	1.604
SWIR – 2	13	1.633	1.688	0.055	1.6605	1.66
SWIR – 3	14	1.6896	1.7411	0.0516	1.7153	1.716
SWIR – 4	15	1.7433	1.7959	0.0526	1.7696	1.77
SWIR – 5	16	1.801	1.8488	0.0479	1.8249	1.83
SWIR – 6	17	1.8544	1.8944	0.04	1.8744	1.876
SWIR – 7	18	1.9018	1.9522	0.0504	1.927	1.928
SWIR – 8	19	1.9526	2.0003	0.0476	1.9764	1.978
SWIR – 9	20	2.0547	2.1026	0.0479	2.0787	2.08

SWIR – 10	21	2.1371	2.1838	0.0468	2.1605	2.162
SWIR – 11	22	2.1864	2.2349	0.0485	2.2107	2.212
SWIR – 12	23	2.2367	2.2841	0.0473	2.2604	2.262
SWIR – 13	24	2.2947	2.3649	0.0701	2.3298	2.32
SWIR – 14	25	2.3645	2.4277	0.0632	2.3961	2.39
MIR – 1	26	3.9823	4.1281	0.1457	4.0552	4.065
MIR – 2	27	3.2144	3.3584	0.144	3.2864	3.295
MIR – 3	28	3.3662	3.5148	0.1486	3.4405	3.455
MIR – 4	29	3.5226	3.6705	0.1479	3.5966	3.61
MIR – 5	30	3.6757	3.8107	0.135	3.7432	3.76
MIR – 6	31	3.8242	3.9776	0.1534	3.9009	3.915
MIR – 7	32	3.9823	4.1281	0.1457	4.0552	4.065
MIR – 8	33	4.1707	4.3236	0.153	4.2472	4.2426
MIR – 9	34	4.3047	4.4576	0.153	4.3812	4.3766
MIR – 10	35	4.4413	4.5825	0.1412	4.5119	4.52
MIR – 11	36	4.5892	4.7373	0.1481	4.6633	4.68
MIR – 12	37	4.7411	4.8887	0.1477	4.8149	4.83
MIR – 13	38	4.89	5.0302	0.1402	4.9601	4.98
MIR – 14	39	5.0321	5.1755	0.1434	5.1038	5.105
MIR – 15	40	5.183	5.3207	0.1376	5.2518	5.26
TIR – 1	41	7.6667	7.9472	0.2805	7.8069	7.83
TIR – 2	42	7.9647	8.3981	0.4333	8.1814	8.25

TIR – 3	43	8.4313	8.7996	0.3683	8.6155	8.65
TIR – 4	44	8.8609	9.2446	0.3837	9.0527	9.05
TIR – 5	45	9.4968	9.8739	0.377	9.6853	9.71
TIR – 6	46	9.9019	10.2764	0.3745	10.0892	10.11
TIR – 7	47	10.3191	10.9292	0.6101	10.6241	10.58
TIR – 8	48	10.9657	11.663	0.6973	11.3144	11.17
TIR – 9	49	11.864	12.3568	0.4929	12.1104	12.06
TIR – 10	50	12.611	13.0864	0.4754	12.8487	12.81

4. Inputs for L-3 ET

The inputs to the STIC algorithm include: i) LST, ii) emissivity, iii) NDVI, iv) albedo, v) net radiation (RN), v) air temperature (T_a), vi) relative humidity (RH), and vii) incoming solar radiation (RG) (Table 1-1). The source of these variables and their derivation is described below.

Table 3 Variables needed for the STIC ET algorithm, and their derivation where applicable.

Variable	Equation / Approach	Source
Land surface temperature (LST)	Temperature-emissivity-separation (TES)	MASTER L-2 LSTE
Broadband Emissivity	TES	MASTER L-2 LSTE
Normalized Difference Vegetation Index (NDVI)	(NIR - RED) / (NIR + RED)	MASTER L-1B Red, SWIR
Albedo	Bonafoni et al. (2020)	MASTER L-1B
Net Radiation (RN)	Verma et al. (2016)	GEOS-5 FP tavg1_2d_rad_Nx (2013 - present) GEOS-5 FP inst3_3d_asm_Np (2013 - present)

		MERRA-2 tavg1_2d_flx_Nx (1998 - present) MERRA-2 inst3_3d_asm_Np (1998 - present) MASTER L-1B MASTER L-2
Air temperature (T_a)	From GEOS-5 / MERRA-2	GEOS-5 FP inst3_3d_asm_Np (2013 - present) MERRA-2 inst3_3d_asm_Np (1998 - present)
Relative humidity (RH)	From GEOS-5 / MERRA-2	GEOS-5 FP inst3_3d_asm_Np (2013 - present) MERRA-2 inst3_3d_asm_Np (1998 - present)

4.1. Land surface temperature and emissivity (LSTE)

The LST and emissivity (ε) estimates are obtained from the MASTER L-2 product which are produced using the TES algorithm as described in Section 1.2.

4.2. NDVI and albedo

Albedo is calculated using MASTER L1B calibrated radiance using the equations from Bonafoni et al. (2020), who present albedo calculation for Sentinel-2. Here we adapt their methodology to the MASTER bands using the following bands (center in microns (μ)) for visible-and-near infrared (VNIR): 0.46, 0.54, 0.66, and for shortwave infrared (SWIR): 0.87, 1.61, 2.16. The albedo (α) is calculated as (1) (Bonafoni et al. (2020):

(1) $\alpha = \sum_{B=1}^{N} \rho B \cdot \omega B$

Where ρ_B is the surface reflectance for a specific band B (as listed above), and ω_B is the weighting coefficient. We use the weighting coefficients as listed in Bonafoni et al. (2020), adapted to the MASTER bands in the VNIR and SWIR.

NDVI is calculated using MASTER L1B calibrated radiance with the equation:

(2) NDVI = (NIR - RED) / (NIR + RED)

Where NIR is reflectance in the near infrared (NIR), and red is reflectance in the visible red band. We use the MASTER band 8 (0.91μ) for NIR, and band 5 (0.66μ) for red visible light. The NIR band was selected to correspond to NIR values used from Landsat for NDVI calculation (https://www.usgs.gov/media/images/landsat-8-band-designations).

4.3. Net radiation (R_N) and Meteorology

Relative humidity (RH) and air temperature (T_a) are derived from the Goddard Earth Observing System - Forward Processing (GEOS-FP) (2013 or later) or Modern-Era Retrospective Analysis for Research and Applications - 2 (MERRA-) data (pre-2013). We use the formulation of net radiation (R_N) from Verma et al. (2016). This formulation is also used in ECOSTRESS Collection 2 Evapotranspiration products (Hook et al., 2024). The computation of R_N is based on calculation of incoming and outgoing radiation fluxes (3) (Verma et al., 2016):

(3) $RN = (R_{SD} - R_{SU}) + (R_{LD} - R_{LU})$

Where R_{SD} is the downwelling shortwave radiation, R_{SU} is the upwelling shortwave radiation, R_{LD} is the downwelling longwave radiation and R_{LU} is the upwelling longwave

radiation. The individual components are described by the following:

R_{SD} is provided by the ancillary meteorological data (either GEOS-FP or MERRA-2).

(4) $R_{SU} = \alpha\ R_{SD}$

(5) $R_{LD} = \sigma\ E_A \varepsilon_a T_a^4$

Where σ is the Stefan-Boltzmann constant (5.67x10-8 W m-2 K-4), ε_a is the atmospheric emissivity, E_A is the vapor pressure (from GEOS-FP or MERRA-2), and T_a is the air temperature (from GEOS-FP or MERRA-2).

(6) $R_{LU} = \sigma \varepsilon_s\ T_s^4$

Where ε_s is the surface emissivity (from the MASTER L2 LSTE) and T_s is surface temperature (LST) from MASTER L2 LSTE.

The coarser meteorology data (MERRA-2, GEOS-FP) are re-gridded to match the MASTER resolution (~50 m). The meteorology quantities are not downscaled in this current methodology, and therefore are spatially coarse compared to the flightlines. The meteorology is linearly interpolated in time by interpolating between two meteorology data points (MERRA-2 or GEOS-FP) to provide estimates closest in time to the acquisition of the flightline.

5. STIC Algorithm: General Form

This section is adapted from the description of the STIC algorithm in the ECOSTRESS Collection 2 ATBD (Hook et al., 2024) and application of STIC to Hyperspectral Thermal Emission Spectrometer (HyTES) (Pascolini-Campbell et al., 2024).

The Surface Temperature Initiated Closure (STIC) (latest version 1.3) is a one-dimensional Surface Energy Balance (SEB) model treating soil-vegetation as a single unit [Mallick et al., 2015; 2018; 2022]. STIC directly integrates LST into the Penman-Monteith Shuttleworth-Wallace system of ET equations (Penman, 1965; Shuttleworth and Wallace, 1985) to solve the aerodynamic temperature ($T0$) - which represents the effective temperature at a height within a canopy where sensible and latent heat fluxes are transferring to the atmosphere. The aerodynamic temperature is the critical temperature for ET modeling. STIC assumes a first-order dependence of aerodynamic conductance (ga) and canopy conductance (gcs) on LST (through soil moisture availability and aerodynamic temperature ($T0$)). Surface moisture availability (also called surface wetness) is first estimated as a function of LST, and then constrains ga and gcs conductances through the surface wetness in an analytical framework.

The inputs to STIC 1.3 include LST (T_s), net radiation (R_N), emissivity (ε_s), albedo (α), NDVI, air temperature (T_a) relative humidity (RH), and incoming solar radiation (RG). The general approach to STIC is (see flow diagram in Figure 2):

i. STIC solves the state equations to find analytical solution of $T0$, and the conductances (ga and gcs).

ii. There are more unknowns in the state equations (e.g., aerodynamic vapor pressure

components), these unknowns are initialized as a function of LST.

iii. The additional unknowns are estimated iteratively by combining Penman-Monteith and Shuttleworth-Wallace equations

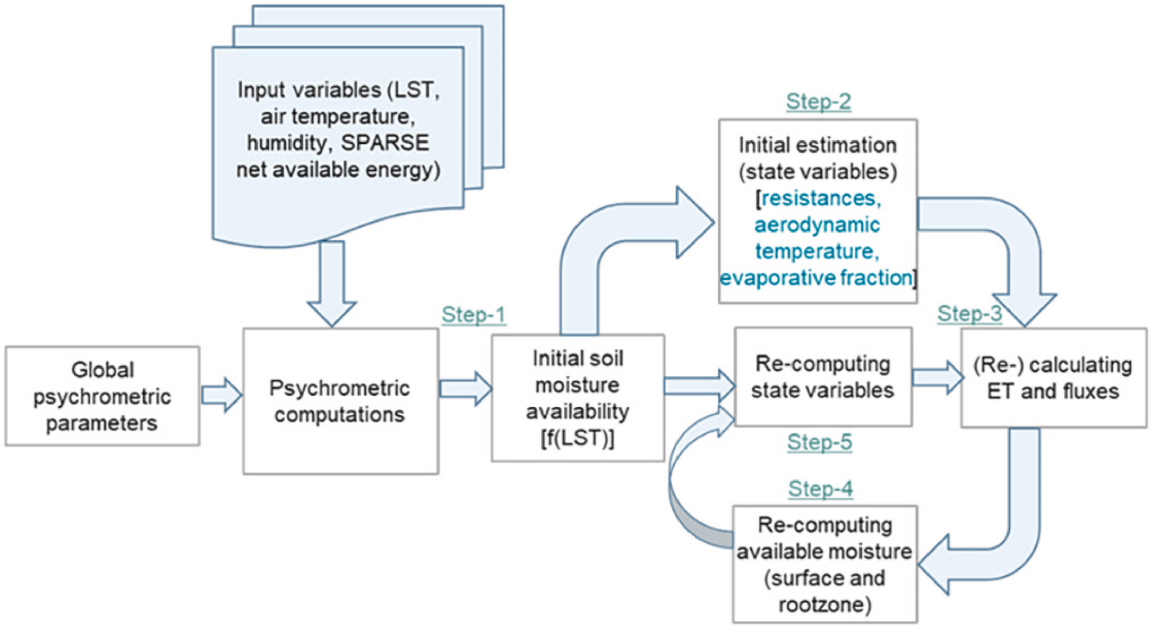

Figure 2. Conceptual flow diagram of the STIC algorithm. For more details see Trebs et al. (2021).

The state equations solved in Step 1 are as follows:

(7) $FE = 2\alpha_{PS}\ 2s + 2\gamma + \gamma(1 + ISM)\ ga\ gcs$

(8) $T0 = Ta + (e0 - ea)\ \gamma\ (1 - FE)\ FE$

(9) $ga = RN - G\ \rho cp\ [(T0 - Ta\ ) + (e0 - ea\ )\ \gamma\ ]$

(10) $gcs = ga\ (e0 - ea)\ (e0 * - e0\ )\ (26)$

Where FE is the evaporative fraction (defined as the fractional contribution of ET from total available energy), α_P is the Priestley-Taylor coefficient [Priestley & Taylor, 1972], s is the slope of the saturation vapor pressure at air temperature (Ta) (hPa/°C), γ is the psychrometric constant (hPa/°C), $e0*$ and $e0$ are the saturation vapor pressure and ambient vapor pressure at the canopy air stream, also called source-sink height (hPa), RN and G are net radiation and ground heat flux (W/m2), ea is the atmospheric vapor pressure (hPa) at the level of Ta measurement, ρ is the air density (kg/m3), and cp is the specific heat of air at constant pressure (j/kg/K).

ISM describes the relative wetness or the intensity of water stress on a surface. This variable controls the transition from potential to actual evaporation, with ISM tending to 1 on an unstressed wet surface, and 0 on a stressed dry surface. Since LST is extremely sensitive to surface water stress variations, it is used directly to estimate ISM. For further details, refer to Mallick et al. (2018, 2022).

In Step 1, initial estimates of an initial estimate of $e0*$, $e0$, ISM, and surface dew point temperature (Tsd), are obtained. The initial ISM and RN are used for an initial estimate of G. In Step 2, initial estimates of the conductances, $T0$, FE and sensible heat (H) and latent heat flux (LE) are obtained. In Step 3, the process is iterated by updating $e0*$, $e0$, ISM, and α, and used to recalculate G, ga, gcs, $T0$, FE, H, and LE until convergence of LE is obtained (~10 – 15 iterations).

Following testing and validation of the STIC algorithm with ECOSTRESS data (Pierrat et al., 2025), we find that the STIC model is highly sensitive to the net available energy (i.e. Rn - G). Using the Bastiaansan et al (1998) method to compute G improves the accuracy of the ET

compared to flux towers, we therefore use this configuration in the adaptation of the STIC model to MASTER data. In this method, G is calculated as:

(11) $G = R_N T_s (0.0038 + 0.0074\alpha)(1 - 0.98^4)$

For its implementation with MASTER data, here we modified the STIC version 1.3 equation in the following ways:

- We use a different method to calculate dew point temperature (Td) with relative humidity (RH) and air temperature (Ta):

(12) $Td = Ta - 100 - RH * 100$

6. MASTER L3 ET Units and Format

The MASTER L3 Evapotranspiration (ET) product is provided (in units of W/m^2). The MASTER L3 ET product is in units W/m^2 and is therefore considered as an energy variable, i.e. latent energy. ET can also be expressed as mass of water evaporated from surfaces and plants, in units of mm/day by applying a conversion using the latent heat of vaporization (MJ/kg).

Fill value for missing data is NaN.

7. Examples of MASTER L3 ET Product Level 3 Evapotranspiration (L3 ET)

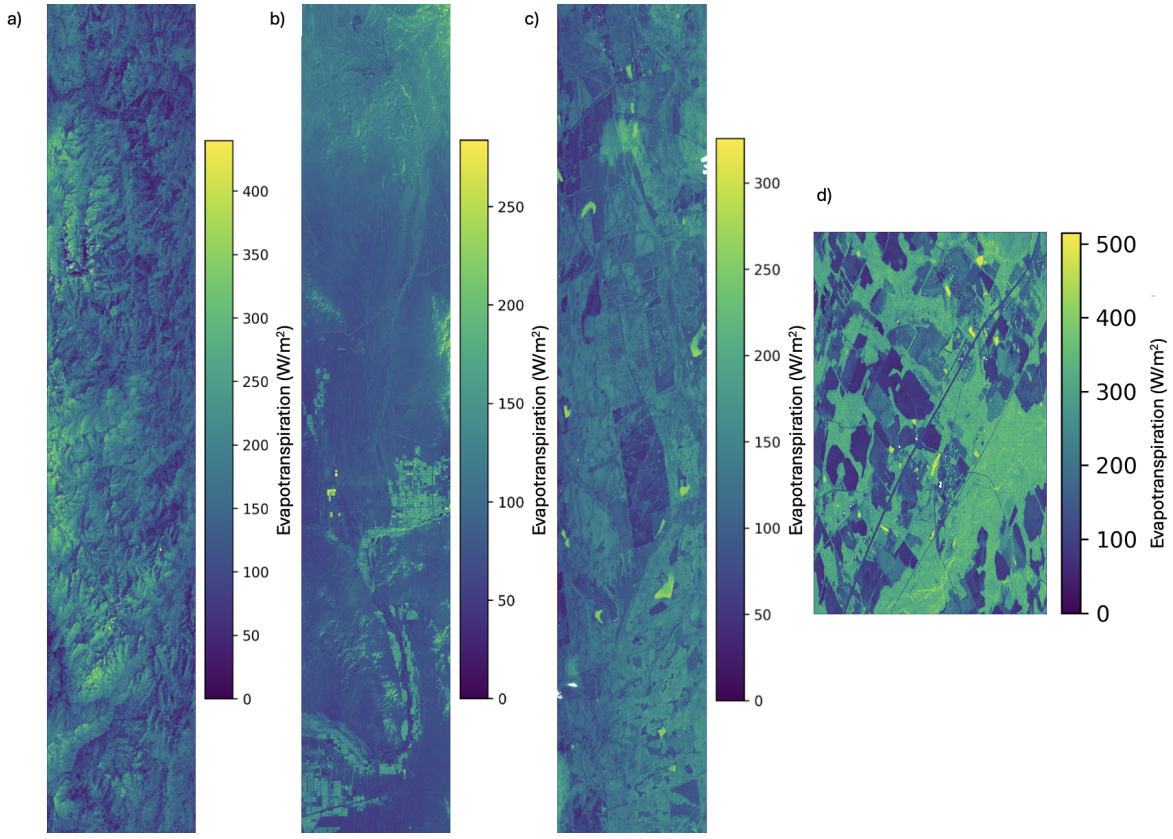

Figure 3. Example of the MASTER L3 evapotranspiration (ET) products (W/m^2) for: a) Northwestern California / Southern Oregon 2024-06-24 (18:41:21), b) Southwestern Arizona (AZ03) 2024-04-03 (18:59:29), c) Alabama / Florida 2025-03-25 (19:08:13) and d) Fort Stewart GA 2025-04-18 (18:12:42). Colormaps represent regions of low (purple) to high (yellow) ET values. Agricultural fields show higher rates of ET compared to adjacent non-agricultural landscapes (b). Dark areas in (d) indicate fields of bare soil with low rates of ET alongside naturally wooded areas.

8. Data Usage

This is Version 0 of the MASTER L3 ET data. We invite comments from the community to improve the current product as we develop the processing framework. We note the following caveats and suggestions when using the data.

MASTER L3 ET has been processed for all MASTER flightlines - including over water and during the night. This may produce erroneous results, as the STIC ET algorithm has not been validated over water. It is also not currently configured to produce ET during the night. We invite users to use the Day/Night information provided in the first column of the MASTER catalog at: https://masterprojects.jpl.nasa.gov/order

9. Metadata

- unit of measurement: Watts per square meter (W m^{-2})
- range of measurement: 0 to 3000 W m^{-2}
- projection: SBG swath
- spatial resolution: variable depending on aircraft and elevation
- temporal resolution: variable depending on flightline acquisition
- spatial extent: variable see https://masterprojects.jpl.nasa.gov/order
- start date time: flightline time, UTC
- end data time: flightline time, UTC
- number of bands: not applicable
- data type: float
- min value: 0
- max value: 3000
- no data value: Nan
- bad data values: Nan
- flags: None

10. Acknowledgements

The research was carried out at the Jet Propulsion Laboratory, California Institute of Technology, under a contract with the National Aeronautics and Space Administration (80NM0018D0004). We thank contributions from the ECOSTRESS Collection 2 Evapotranspiration ATBD. © 2026. California Institute of Technology. Government sponsorship acknowledged.

References

Bastiaanssen, W. G., Pelgrum, H., Wang, J., Ma, Y., Moreno, J. F., Roerink, G. J., & Van der Wal, T. (1998). A remote sensing surface energy balance algorithm for land (SEBAL).: Part 2: Validation. *Journal of hydrology*, *212*, 213-229.

Bonafoni, S., & Sekertekin, A. (2020). Albedo retrieval from Sentinel-2 by new narrow-to-broadband conversion coefficients. *IEEE Geoscience and Remote Sensing Letters*, *17*(9), 1618-1622.

Gillespie, A., Rokugawa, S., Matsunaga, T., Cothern, J. S., Hook, S., & Kahle, A. B. (1998). A temperature and emissivity separation algorithm for Advanced Spaceborne Thermal Emission and Reflection Radiometer (ASTER) images. *IEEE transactions on geoscience and remote sensing*, *36*(4), 1113-1126.

Hook, S. J. Myers, J. J., Thome, K. J., Fitzgerald, M. and A. B. Kahle, 2001. The MODIS/ASTER airborne simulator (MASTER) - a new instrument for earth science studies. Remote Sensing of Environment, vol. 76, Issue 1, pp. 93-102.

Hook, S., Cawse-Nicholson, K., Halverson, G., Hatch, B., Johnson, M., Pascolini-Campbell, M., Purdy, A. J., Sikka, M., Villanueva-Weeks, C., (2024) Level-3 Evapotranspiration L3 (JET) Algorithm Theoretical Basis Document. JPL Publication - D-94645. Available online: https://ecostress.jpl.nasa.gov/downloads/atbd/ECOSTRESS_L3_JET_ATBD_20240719v1-1.pdf

King, M. D., Menzel, W. P., Grant, P. S., Myers, J. S., Arnold, G. T., Platnick, S. E., ... & Osterwisch, F. G. (1996). Airborne scanning spectrometer for remote sensing of cloud, aerosol, water vapor, and surface properties. *Journal of Atmospheric and Oceanic Technology*, *13*(4), 777-794.

Mallick, K., Boegh, E., Trebs, I., Alfieri, J. G., Kustas, W. P., Prueger, J. H., ... & Jarvis, A. J. (2015). Reintroducing radiometric surface temperature into the Penman-Monteith formulation. *Water Resources Research*, *51*(8), 6214-6243.

Mallick, K., Toivonen, E., Trebs, I., Boegh, E., Cleverly, J., Eamus, D., ... & Garcia, M. (2018). Bridging thermal infrared sensing and physically-based evapotranspiration modeling: From theoretical implementation to validation across an aridity gradient in Australian ecosystems. *Water Resources Research*, *54*(5), 3409-3435.

Mallick, K., Baldocchi, D., Jarvis, A., Hu, T., Trebs, I., Sulis, M., ... & Kustas, W. P. (2022). Insights Into the Aerodynamic Versus Radiometric Surface Temperature Debate in Thermal-Based Evaporation Modeling. Geophysical Research Letters, 49(15), e2021GL097568. doi: https://doi.org/10.1029/2021GL097568

Monteith, J. L. (1965). Evaporation and environment. In *Symposia of the society for experimental biology* (Vol. 19, pp. 205-234). Cambridge University Press (CUP) Cambridge.

Pascolini-Campbell, M., Hook, S., Mallick, K., Langsdale, M., Hulley, G., Cawse-Nicholson, K., ... & Rabuffi, F. (2024). A first assessment of airborne HyTES-based land surface temperature and evapotranspiration. *Remote Sensing Applications: Society and Environment*, *36*, 101344.

Penman, H. L. (1948). Natural evaporation from open water, bare soil and grass. *Proceedings of the Royal Society of London. Series A. Mathematical and Physical Sciences*, *193*(1032), 120-145.

Shuttleworth, W. J., & Wallace, J. S. (1985). Evaporation from sparse crops-an energy combination theory. *Quarterly Journal of the Royal Meteorological Society*, *111*(469), 839-855.

Trebs, I., Mallick, K., Bhattarai, N., Sulis, M., Cleverly, J., Woodgate, W., ... & Boulet, G. (2021). The role of aerodynamic resistance in thermal remote sensing-based evapotranspiration models. *Remote Sensing of Environment*, *264*, 112602.

Verma, M., Fisher, J. B., Mallick, K., Ryu, Y., Kobayashi, H., Guillaume, A., ... & Cescatti, A. (2016). Global surface net-radiation at 5 km from MODIS Terra. *Remote Sensing*, *8*(9), 739.